Materials Research Proceedings 54 (2025) 313-321 https://doi.org/10.21741/9781644903599-34

Meso- and macroscale modelling strategies for biomimetic structures produced using L-PBF technology

Anastasia Ciccarella[1,a *], Giuseppe Dell'Avvocato[1,b], Gabriele Cortis[2,c], Daniele Cortis[3,d], Donato Orlandi[3,e], Luca di Angelo[1,f], Luca Cortese[2,g] and Edoardo Mancini[1,h]

[1]Università degli Studi dell'Aquila, DIIIE, Piazzale Ernesto Pontieri I, 67100 L'Aquila, Italy

[2]Sapienza University of Rome, DIMA, 00184 Rome, Italy

[3]Istituto Nazionale di Fisica Nucleare, Laboratori Nazionali del Gran Sasso, via G. Acitelli 22, 67100 L'Aquila, Italia

[a]anastasia.ciccarella@graduate.univaq.it, [b]giuseppe.dellavvocato@univaq.it, [c]gabriele.cortis@uniroma1.it, [d]daniele.cortis@lngs.infn.it, [e]donato.orlandi@lngs.infn.it, [f]luca.diangelo@univaq.it, [g]luca.cortese@uniroma1.it, [h]edoardo.mancini@univaq.it

Keywords: Biomimetic, L-PBF, TPMS, Anisotropy, Meso and Macroscale

Abstract. This paper investigates the mechanical behaviour of biomimetic structures produced using L-PBF technology. Specifically, the triply periodic minimal surface (TPMS) gyroid structure was analysed. The TPMS are receiving significant attention in biomedical applications to produce structures with high strength-to-weight ratio, better control over the transition in properties between the prosthesis and the bone tissue, such as stiffness and density, and improved interface adhesion. The mechanical characterisation of these structures is the current challenge for researchers. We propose a preliminary modelling strategy for a homogenisation procedure based on the Representative Volume Element (RVE) theory and traditional mesoscale and macroscale finite element (FE) analysis integrated with evaluating the anisotropy induced by the printing process. The results indicate that the L-PBF produces an orthotropic base material, the unit cell exhibits an anisotropic behaviour, and the macroscopic modelling reduces the computational cost. However, a mesoscopic approach is necessary to define the anisotropic elastic matrix of the cell.

Introduction

In millions of years of evolution, nature has created countless complex structures, endowing organisms with unique and superior characteristics [1].

As a source of conceptual design inspiration, nature develops structural systems with optimum morphology, the least energy consumption, and well-adaptation of the surroundings. One of the main examples of the natural optimum design are cellular structures, such as bone, butterfly wings and beehive [2]. Among these, bone is particularly interesting for its lightness and high specific strength, thanks to the coexistence of a cortical structure and a trabecular one.

Researchers are focused on designing and manufacturing structures that mimic nature, known as biomimetic structures. In orthopaedic industry, the ability to replace natural structures can offer specific properties: high strength-to-weight ratio, decreased stress-shielding, better control over the transition in properties between the prosthesis and the bone tissue, such as stiffness and density, and improvement interface adhesion [3, 4]

Biomimetic structures can be produced through Additive Manufacturing technologies, which have enabled the production of complex structures with high-performance base materials [5]. Nevertheless, the use of biomimetic structures is limited due to a lack of knowledge of their mechanical behaviour. The mechanical properties of biomimetic structures can be studied numerically by analysing the unit cell (mesoscale modelling) or using a homogeneous material model (macroscale modelling) [6]. The adoption of mesoscopic modelling usually determines a high computational cost, so the ability to use a homogeneous material model that can reproduce biomimetic behaviour may overcome this limitation [7, 8]. For this reason, meso- and macroscale modelling strategies for biomimetic structures produced by L-PBF are proposed. The primary objectives are to assess the mechanical behaviour of biomimetic structures, streamline the design and analysis of components using these structures, and lower computational costs.

Considering that L-PBF technology induces an orthotropic behaviour [9], assessing the degree of anisotropy is necessary. Seeing as the bulk material properties influence the mechanical response of biomimetic structures, if the base material exhibits anisotropic behaviour induced by the printing process, this, in turn, leads to anisotropic biomimetic structure.

This study focuses on the gyroid structure in Fe-3171. The gyroid structure typically exhibits isotropic behaviour within a relative density range of 0.2 to 0.6 [5]. Therefore, it is important to investigate how the base material's anisotropy influences the structure's overall behaviour. Consequently, a double anisotropy effect has been examined and integrated into the modelling strategy. The experimental-numerical procedure addresses the study.

Material and method

Material. The material tested is a hardening steel (Fe-3171) whose typical characteristics of tensile test, for relative density > 99.9%, are reported in Table 1 [8].

Table 1 – Tensile test material characteristics [8]

	Tensile strength Rm [N/mm^2]	Yield strength Re [N/mm^2]	Elongation at break A [%]
As built	1095	1040	10

All specimens, as shown in Fig. 1, have been produced considering two different orientations to the Z-building direction: printing direction 0° also indicated with Z, and normal direction 90° marked with X. A SISMA MySint100 PM/RM machine equipped with a single InfraRed (IR) laser was used.

Figure 1 – Produced tensile (a) prismatic, (b) dog-bone and (c) torsion specimens: 0° (Z), 90°(X) orientation respect to z-direction

The labels of the samples tested in quasi-static (QS) conditions are reported in Table 2.

Table 2 – Labels' specimens for tests

Test type	Specimen label	Printing direction	Loading direction
QS tensile test	CVi	Z	Z
QS tensile test	COi	Z	X
QS tensile test	PVi	Z	Z
QS tensile test	POi	Z	X
QS torsion test	TV	Z	Z
QS torsion test	TO	Z	X

Hydrostatic balance was used to measure the relative density of the samples. The measurement results are shown in Fig. 2.

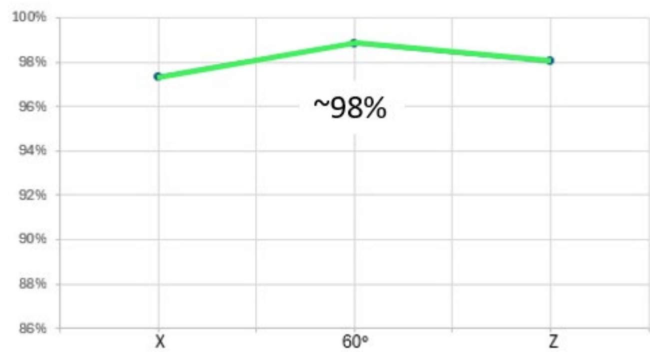

Figure 2 – Relative density measurements as a function of printed direction

Equipment**.** Quasi-static tensile tests were performed by a universal servo-hydraulic MTS with a maximum axial load of 250kN available at "Sapienza" University of Rome (Fig. 3a) and by a traditional universal tensile machine available at the University Study of L'Aquila (Fig. 3b). A custom biaxial tension-torsion equipment available at "Sapienza" University of Rome was used for the torsion quasi-static tests (Fig. 3c). FLIR cameras were also used to acquire and analyse images during the tensile tests.

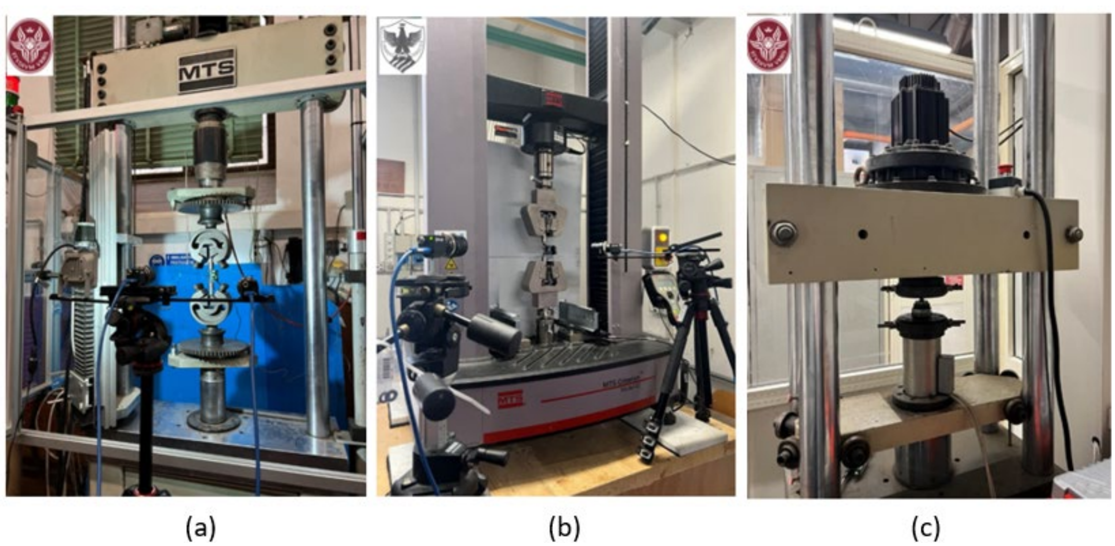

Figure 3 – Equipment for (a, b) tensile and (c) torsion tests

Method. Initial experimental tests were conducted to evaluate the mechanical properties induced by L-PBF on the base material, determining the elastic matrix of the base material ($\boldsymbol{E_{base}}$, Fig. 4).

Materials Research Proceedings 54 (2025) 313-321 https://doi.org/10.21741/9781644903599-34

$$\begin{bmatrix} 1/E_1 & -\nu_{21}/E_2 & -\nu_{31}/E_3 & & & \\ -\nu_{12}/E_1 & 1/E_2 & -\nu_{32}/E_3 & & 0 & \\ -\nu_{13}/E_1 & -\nu_{23}/E_2 & 1/E_3 & & & \\ & & & 1/G_{12} & & \\ & 0 & & & 1/G_{23} & \\ & & & & & 1/G_{13} \end{bmatrix}$$

Figure 4 – Elastic matrix E_{base}

Subsequently, a numerical homogenisation procedure based on the Representative Volume Element (RVE) theory was performed. As RVE, an 8x8x8 mm gyroid unit cell with a thickness of 1 mm and $\rho_{relative} \sim 0.365$ was analysed, as shown in Fig. 5.

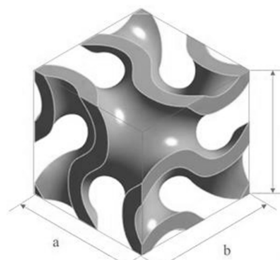

Figure 5 – RVE Gyroid with a thickness of 1mm

A mesoscopic numerical model was prepared on the unit cell to identify the elastic matrix of the unit cell ($\boldsymbol{E_{cell}}$). The material properties assigned to the unit cell correspond to the elastic matrix of the base material $\boldsymbol{E_{base}}$ obtained experimentally. The periodic boundary conditions were applied to the unit cell model according to [10], avoiding the over-constraining of the RVE. Six displacement cases, shown in Fig. 6, were applied individually on the cell surfaces.

$$\varepsilon_{11} = [0.02,0,0,0,0,0]^T \quad \varepsilon_{22} = [0,0.02,0,0,0,0]^T \quad \varepsilon_{33} = [0,0,0.02,0,0,0]^T$$
$$\varepsilon_{12} = [0,0,0,0.02,0,0]^T \quad \varepsilon_{23} = [0,0,0,0,0.02,0]^T \quad \varepsilon_{31} = [0,0,0,0,0,0.02]^T$$

Figure 6 – Six loading conditions [11]

The values of the stress tensor $\boldsymbol{\sigma}$ were calculated from the reaction force. According to Hooke's law (Eq. 1), the elastic matrix of the unit cell $\boldsymbol{E_{cell}}$ (Fig. 7) was obtained.

$$\{\sigma\} = [E]\,\{\varepsilon\}. \quad (1)$$

$$\begin{bmatrix} E_{11} & E_{12} & E_{13} & E_{14} & E_{15} & E_{16} \\ & E_{22} & E_{23} & E_{24} & E_{25} & E_{27} \\ & & E_{33} & E_{34} & E_{35} & E_{36} \\ & & & E_{44} & E_{45} & E_{46} \\ & \text{Symmetric} & & & E_{55} & E_{56} \\ & & & & & E_{66} \end{bmatrix}$$

Figure 7 – Elastic matrix of the unit cell $\boldsymbol{E_{cell}}$

Components E_{11}, E_{12} and E_{44} can be used to evaluate the anisotropy of the unit cell through Zener ratio Z [12], expressed by Eq. 2.

$$Z = \frac{2E_{44}}{E_{11}-E_{12}}. \quad (2)$$

If Z is close to one, the structure can be considered as isotropic.

To verify the numerical homogenisation, mesoscale and macroscale FE analyses were conducted on 8x8x8 mm gyroid and cubic cells. The elastic matrix $\boldsymbol{E_{base}}$ was assigned as material property for the mesoscale, while the elastic matrix $\boldsymbol{E_{cell}}$ was used for the macroscale. In both analyses, displacement case and compression-only support were applied, as shown in Fig. 8, to determine the stiffness of the cells.

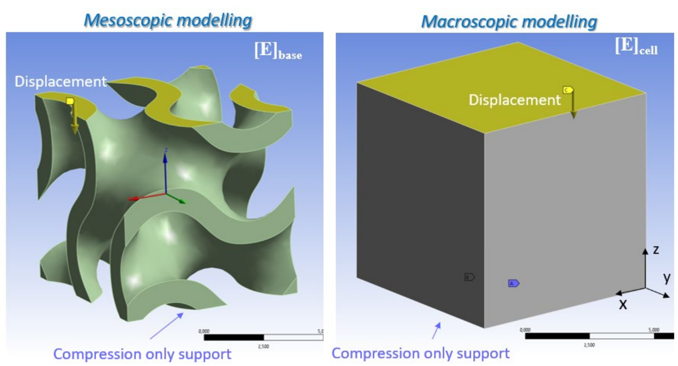

Figure 8 – Boundary condition on mesoscale and macroscale simulations

The RVE model was discretized using 4-node linear tetrahedral elements with an average element size of 0.1 mm (Fig. 9). The mesh size was selected following a sensitivity analysis on the mesh size conducted in [5]. The cubic cell was discretized using linear tetrahedral elements with an average size of 0.6 mm.

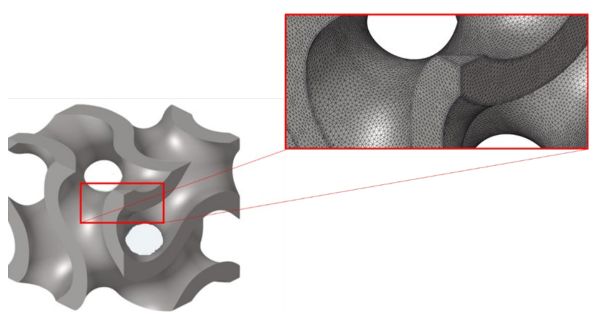

Figure 9 – Mesh RVE

Results and discussion

Experimental results. The engineering stress-strain curves for quasi-static tensile tests are illustrated in Fig.10.

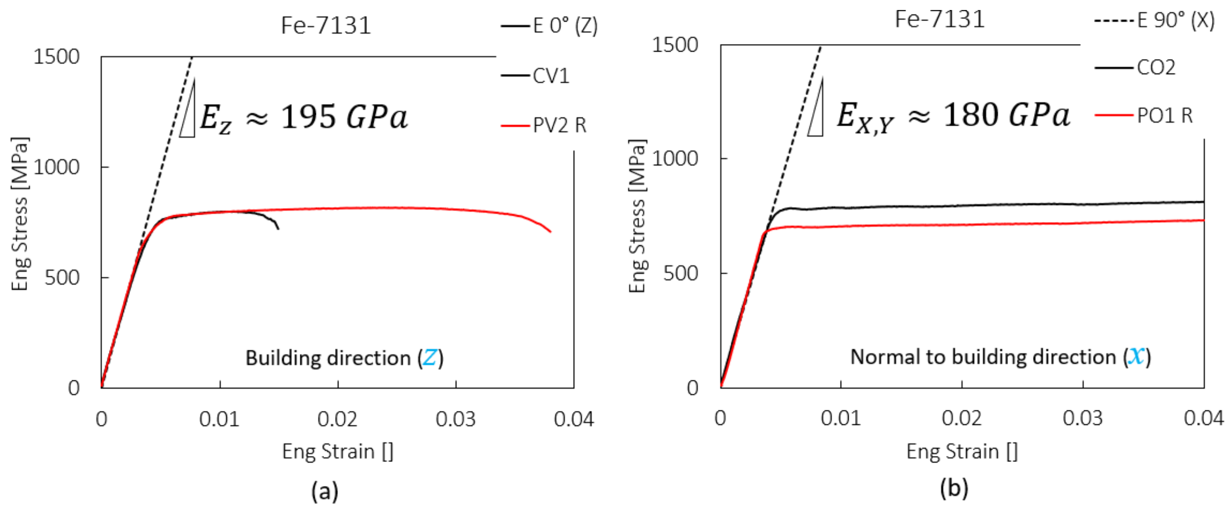

Figure 10 – Engineering stress-strain for quasi-static tensile tests: (a) loading direction Z (b) loading direction X

The differential $\Delta_{QS}(E_z E_x) \approx 15GPa$ demonstrates the anisotropy induced by printing direction, according to [5]. The dispersion between the behaviour of prismatic and dog-bone samples produced normal to the building direction (Fig. 10b) can be attributed to manufacturing defects. These results require further investigation. The torque-angle rotation curves for quasi-static torsion tests are shown in Fig. 11.

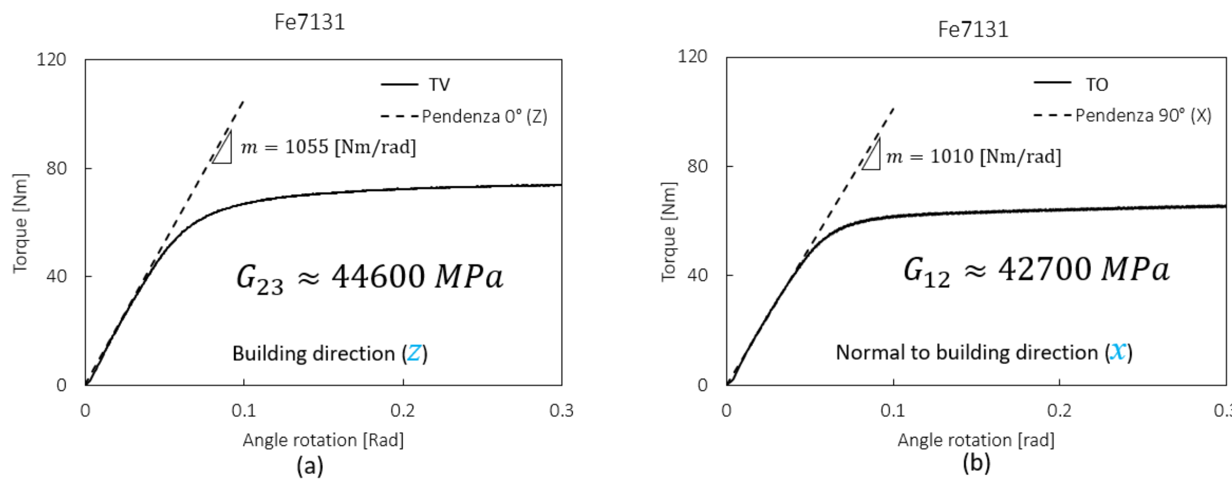

Figure 11 – Experimental results for torsion tests: (a) loading direction Z (b)loading direction X

These curves permit the shear modulus G calculation. To determine the Poisson's ratio, the transverse strain was measured by analysing the recorded images, while the longitudinal strain was obtained using an extensometer.

The experimental results are summarised in Table 3, where $1 \equiv X, 2 \equiv Y, 3 \equiv Z$. The mechanical behaviour on plane XY is consistent. The material exhibits a transverse isotropy mechanical behaviour.

Table 3 – Experimental quasi-static results

$E_1 = E_2 = E$	180000 MPa
E_3	195000 MPa
ν_{31}	0.279
$\nu_{23} = \nu_{13}$	0.285
ν_{12}	0.319
G_{12}	42700
$G_{23} = G_{13} = G$	44600

Numerical results. The numerical homogenisation results are expressed in terms of the elastic matrix $\boldsymbol{E_{cell}}$ (Fig. 12), which is needed for the macroscale modelling.

23232.8	8759.4	8712.5	6.9	400.7	6.9
	23332.0	8737.5	10.7	10.4	398.3
		24073.4	415.6	9.1	10.5
			6391.6	0.1	11.8
				6511.9	-0.7
					6532.3

Figure 12 – Numerical homogenisation results in terms of $\boldsymbol{E_{cell}}$

The Zener ratio was found to be 0.88. Contrary to what concerns the literature [13], the gyroid structure exhibited anisotropic behaviour due to the anisotropy of the base material induced by L-PBF.

The numerical homogenisation was verified by comparing additional meso- and macroscale simulations described in the material and method section.

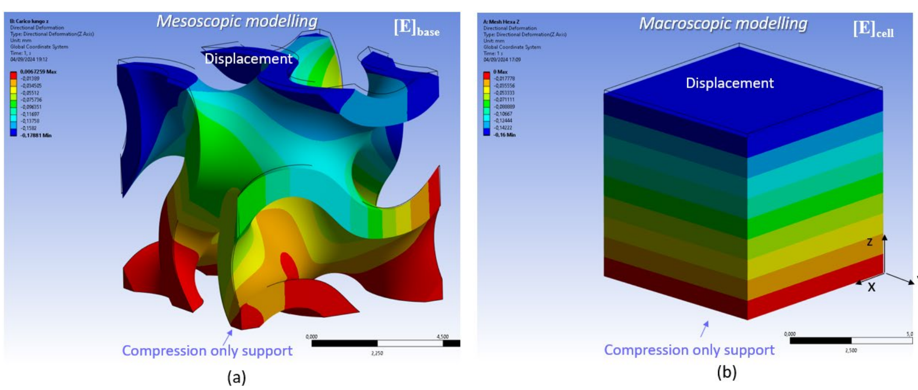

Figure 13 – Numerical (a) meso- and (b) macroscale modelling results

The stiffness of the gyroid cell (Fig. 13a) is 143 kN/mm. Instead, the cube's stiffness (Fig. 13b) is 148 kN/mm. The results are consistent, but the macroscale approach, using a homogeneous material model, reproduces the behaviour of the gyroid with a lower computational cost.

Conclusions

A preliminary meso- and macroscale modelling strategy for the gyroid structure was made, integrating the evaluation of the anisotropy induced by the printing process in Fe-3171 steel. The L-PBF technology produces an orthotropic base material. The calculation of the elastic matrix $\boldsymbol{E_{base}}$ is achieved by printing samples along the orthotropy directions. The base material's anisotropy influences the gyroid cell's mechanical behaviour, as confirms the Zener ratio.

The meso- and macroscale results highlighted the ability of the homogeneous material model to study biomimetic structures, drastically reducing the computational cost. However, mesoscopic modelling is necessary to define the anisotropic elastic matrix of the unit cell.

To conclude, this study requires further investigations. Future research will focus on analysing the dispersion of the specimens loaded in the X direction, studying the mechanical behaviour under compression, and performing dynamic tests. These efforts aim to make the procedure more comprehensive and robust, including a detailed evaluation of how the base material's anisotropy influences the gyroids' behaviour.

Funding

Funded by the European Union - Next Generation EU. Views and opinions expressed are however those of the author(s) only and do not necessarily reflect those of the European Union or the European Commission. Neither the European Union nor the European Commission can be held responsible for them.

PNRR MUR M4 C2 Inv. 1.5 CUP B83C22003920001 - ORTO ATTIVE

References

[1] J. Li, M. Li, J. J. Koh, J. Wang, and Z. Lyu, "3D-printed biomimetic structures for energy and environmental applications," *DeCarbon*, vol. 3, p. 100026, Mar. 2024. https://doi.org/10.1016/j.decarb.2023.100026.

[2] S. Ataollahi, "A review on additive manufacturing of lattice structures in tissue engineering," Nov. 01, 2023, *Elsevier B.V. https://doi.org/*10.1016/j.bprint.2023.e00304.

[3] E. Alabort, D. Barba, and R. C. Reed, "Design of metallic bone by additive manufacturing," *Scr Mater*, vol. 164, pp. 110–114, Apr. 2019. https://doi.org/10.1016/j.scriptamat.2019.01.022.

[4] L. Mullen, R. C. Stamp, W. K. Brooks, E. Jones, and C. J. Sutcliffe, "Selective laser melting: A regular unit cell approach for the manufacture of porous, titanium, bone in-growth constructs, suitable for orthopedic applications," *J Biomed Mater Res B Appl Biomater*, vol. 89, no. 2, pp. 325–334, May 2009. https://doi.org/10.1002/jbm.b.31219.

[5] E. Mancini, M. Utzeri, E. Farotti, A. Lattanzi, and M. Sasso, "DLP printed 3D gyroid structure: Mechanical response at meso and macro scale," *Mechanics of Materials*, vol. 192, May 2024. https://doi.org/10.1016/j.mechmat.2024.104970.

[6] D. W. Abueidda, M. Bakir, R. K. Abu Al-Rub, J. S. Bergström, N. A. Sobh, and I. Jasiuk, "Mechanical properties of 3D printed polymeric cellular materials with triply periodic minimal surface architectures," *Mater Des*, vol. 122, pp. 255–267, May 2017. https://doi.org/10.1016/j.matdes.2017.03.018.

[7] M. Smith, Z. Guan, and W. J. Cantwell, "Finite element modelling of the compressive response of lattice structures manufactured using the selective laser melting technique," *Int J Mech Sci*, vol. 67, pp. 28–41, 2013. https://doi.org/10.1016/j.ijmecsci.2012.12.004.

[8] E. Mancini *et al.*, "High strain rate investigation on the mechanical anisotropy induced by SLM technology on a 3D printed steel," in *Materials Research Proceedings*, Association of American Publishers, 2024, pp. 2220–2225. https://doi.org/10.21741/9781644903131-244.

[9] A. Charmi *et al.*, "Mechanical anisotropy of additively manufactured stainless steel 316L: An experimental and numerical study," *Materials Science and Engineering: A*, vol. 799, Jan. 2021. https://doi.org/10.1016/j.msea.2020.140154.

[10] Z. Xia, Y. Zhang, and F. Ellyin, "A unified periodical boundary conditions for representative volume elements of composites and applications," *Int J Solids Struct*, vol. 40, no. 8, pp. 1907–1921, 2003. https://doi.org/10.1016/S0020-7683(03)00024-6.

[11] E. Mancini, M. Utzeri, and M. Sasso, "Investigation on Homogeneous Modeling of Gyroid Lattice Structures: Numerical Study in Static and Dynamic Conditions," in *Key Engineering Materials*, Trans Tech Publications Ltd, 2022, pp. 2119–2126. https://doi.org/10.4028/p-3561q0.

[12] C.M. Zener, S. Siegel, Elasticity and Anelasticity of Metals, J. Phys. Colloid Chem. 53 (1949) 1468–1468. https://doi.org/10.1021/j150474a017.

[13] C. Chatzigeorgiou, B. Piotrowski, Y. Chemisky, P. Laheurte, and F. Meraghni, "Numerical investigation of the effective mechanical properties and local stress distributions of TPMS-based and strut-based lattices for biomedical applications," *J Mech Behav Biomed Mater*, vol. 126, Feb. 2022. https://doi.org/10.1016/j.jmbbm.2021.105025.